

# The Effect of Intrinsic UV Absorbers on the Ionizing Continuum and Narrow Emission Line Ratios in Seyfert Galaxies

S. B. Kraemer<sup>1,4</sup>, T. J. Turner<sup>2,3</sup>, D. M. Crenshaw<sup>1</sup>, & I. M. George<sup>2</sup>

Received Sept. 23, 1998; accepted Jan. 21, 1999

to appear in *The Astrophysical Journal*

---

<sup>1</sup>Catholic University of America, NASA/Goddard Space Flight Center, Code 681, Greenbelt, MD 20771.

<sup>2</sup>Universities Space Research Association, NASA/Goddard Space Flight Center, Code 660, Greenbelt, MD 20771.

<sup>3</sup>Present address, University of Maryland, Baltimore County

<sup>4</sup>Email: stiskraemer@yancey.gsfc.nasa.gov.

## ABSTRACT

We explore the effects of UV absorbing material on the shape of the EUV continuum radiation emitted by the active galactic nucleus, and on the relative strengths of emission lines, formed in the narrow line regions of Seyfert galaxies, excited by this continuum. Within a sample of Seyfert 1.5 galaxies, objects with flatter soft X-ray slopes tend to have lower values of He II  $\lambda 4686/\text{H}\beta$ , which implies a correlation between the observed spectral energy distribution of the ionizing continuum and the narrow emission line strengths. Objects with the flattest soft X-ray continua tend to possess high column density UV absorption and it is plausible that the differences in narrow emission line ratios among these galaxies are an indication of the effects of absorbing material internal to the narrow line region, rather than intrinsic differences in continuum shape. We have generated a set of photoionization models to examine the effect of a range of UV absorbers on the ionizing continuum and, hence, the resulting conditions in a typical narrow line cloud. Our results indicate that a low ionization UV absorber with large covering factor will indeed produce the combination of narrow line ratios and soft X-ray spectral characteristics observed in several Seyfert 1.5 galaxies. Our results also suggest that low ionization UV absorption may be more common than currently believed.

*Subject headings:* galaxies: Seyfert - X-rays: galaxies

## 1. Introduction

Since the launch of *IUE* in 1978, it has been known that the UV spectra of a few Seyfert galaxies show absorption lines that are thought to be intrinsic to the nucleus, as evidenced by their large radial velocities relative to the host galaxy, large widths, and variability. Although *IUE* studies revealed few Seyfert 1 galaxies that showed intrinsic absorption (Ulrich 1988), an examination of *HST* spectra, with better sensitivity and/or resolution, reveals that more than half ( $\sim 60\%$ ) of these galaxies showed such absorption (Crenshaw et al. 1998). Also, approximately half of a sample of Seyfert 1 galaxies observed in X-rays show the presence of an X-ray (“warm”) absorber, characterized by absorption edges of O VII and O VIII (Reynolds 1997; George et al. 1998a). Although there have been suggestions that the UV and X-ray absorbers are physically linked (cf. Mathur, Elvis, & Wilkes 1995; George et al. 1998a), it is also possible that the absorbing material is comprised of different components at different radial distances from the central source. In any case, it is clear that the absorbing material is an important physical component in the inner regions of Seyfert galaxies and is likely to have a global covering factor between 0.5 and 1.0 (Crenshaw et al. 1998).

It follows that if the covering factor of the absorbing material is large, or, at least, co-planar with the narrow-line region (NLR), its presence will alter the spectral energy distribution (SED) of the ionizing continuum to which the NLR gas is exposed. The effect of the absorption on the ionizing continuum depends on the ionization state of the absorber since the conditions in the NLR gas will depend principally on the number of photons between 13.6 and 100 eV, where the cross-sections of H, He I and He II are greatest. A highly ionized X-ray absorber may be transparent at energies below the O VII edge ( $\sim 740$  eV), unless it is Compton thick. In such a case, the NLR will be illuminated by an SED that is effectively intrinsic. On the other hand, a UV absorber with sufficient column

density to produce absorption lines of Ly $\alpha$ , N V  $\lambda$  1240, and C IV  $\lambda$  1550 may also produce a significant edge at the He II Lyman limit. In this case, the effect on the conditions in the NLR may be significant, and will be revealed by the ratios of emission lines, particularly He II  $\lambda$ 4686/H $\beta$  which is especially sensitive to the SED of the ionizing continuum. If absorption from lower ionization states, in particular Mg II  $\lambda$ 2800, is present, there may be significant absorption of continuum photons near the hydrogen Lyman limit as well. As the attenuation below 100 eV becomes greater, the average ionization state of the NLR will drop, while at the same time ionization and heating by X-rays may dominate, resulting in zones of warm ( $T \sim 10^4$ K), partially ionized gas.

In order to examine the possible effects of a low ionization UV absorber on the ionizing SED and NLR, we have generated a set of photoionization models. The photoionization code used in this study was developed by Kraemer (1985) and has been described in detail in several previous papers (cf. Kraemer et al. 1994). This code has a high energy cutoff at 5 keV. This is a sufficiently high cutoff energy to model the effects in the low ionization gas, although may be inadequate for an X-ray absorber model. The modeling methodology and results are discussed in detail in the following sections.

## 2. The Models

### 2.1. Setting up the Model

The purpose of this phase of the modeling is to determine how the modification of the SED varies for different column densities of the principle UV absorbers. While the physical conditions within the absorbing gas are of interest, their examination is not the principle part of this study. Therefore, we have taken a very simple approach, and held most parameters fixed while generating the absorber models.

The concept that absorption by intervening gas can modify the ionizing continuum to which the NLR gas is exposed is far from new. The most detailed treatment has been that of Ferland & Mushotzsky (1982), in which they modeled the NLR of NGC 4151, assuming it was ionized by a continuum modified by a “leaky absorber”. In this model, broad line region (BLR) clouds, effectively opaque to the ionizing continuum at EUV energies, cover 90% of the source, while the remaining 10% of the ionizing continuum escapes unattenuated. However, their absorber models predicted ionic column densities several orders of magnitude larger than those calculated from recent observations of NGC 4151 (cf. Weymann et al. 1997), and the details of X-ray absorption were not well known at the time the paper was written. Therefore, it seems worthwhile to revisit this approach, with the benefit of better constraints on the absorbers.

In order to generate these models, we had to assume an intrinsic SED for the ionizing continuum. Unfortunately, absorption by galactic neutral hydrogen makes it all but impossible to get a measurement of the SED in the EUV for the vast majority of AGN, and, thus, there is no direct way to determine the intrinsic shape of the ionizing continuum. Although there has been significant effort directed towards understanding the shape of the ionizing continuum in active galactic nuclei (AGN), no consensus has been reached. Recent work by Zheng et al. (1997) and Laor et al. (1997) suggest that, for QSOs at intermediate redshift, the ionizing continuum from the Lyman limit to soft X-ray energies may be characterized by a power law, with an index  $\alpha \approx -2$ . While some lower luminosity AGN, specifically Seyfert galaxies, are similar, others may have somewhat flatter indices ( $\alpha \approx -1.5$ ; Korista, Ferland, & Baldwin 1997). Korista et al. (1997) have shown that a spectral energy distribution (SED) similar to the composite QSO spectrum proposed by Zheng et al. (1995) does not possess sufficient He II ionizing photons to produce the observed equivalent width of the broad He II  $\lambda 1640$  emission lines in the Seyfert 1 galaxy Mrk 335 (specifically) and, perhaps, AGN in general. Mathews & Ferland (1987) have proposed that the bulk of

the necessary He II ionizing photons in AGN could arise from the so-called “big blue bump” (BBB) (cf. Malkan 1983). Therefore, we have generated two sets of models. For the first, which we will call the “power-law” SED, we assumed a broken power law,  $F_\nu = K\nu^\alpha$  where:

$$\alpha = -1.5, \quad 13.6\text{eV} \leq h\nu < 1000\text{eV} \quad (1)$$

$$\alpha = -0.7, \quad h\nu \geq 1000\text{eV}. \quad (2)$$

For the other SED, which we will call the “BBB” SED, we adopted the parameterization of the Mathews & Ferland continuum given in Laor et al. (1997), where

$$F_\nu = K\nu^{\alpha_0} e^{h\nu/KT_{cut}} \quad (3)$$

where,  $\alpha_0 = -0.3$  and  $T_{cut} = 5.4 \times 10^5\text{K}$ . At energies  $\geq 200\text{ eV}$ ,  $F_\nu = K\nu^\alpha$ , with

$$\alpha = -2, \quad 200\text{eV} \leq h\nu < 1000\text{eV} \quad (4)$$

$$\alpha = -0.7, \quad h\nu \geq 1000\text{eV}. \quad (5)$$

Although it is certainly likely that there is greater variation in the intrinsic SED among Seyfert galaxies, one can obtain a qualitative understanding of how conditions would vary with other power laws and/or differing BBB contributions from these results.

There have been several attempts to determine the density of the gas in which the UV resonance line absorption arises. Density estimates based on recombination timescale arguments are typically  $\geq 10^5 \text{ cm}^{-3}$  (cf. Voit et al. 1987; Shull & Sachs 1993). The presence of weak absorption from excited states in the spectrum of NGC 4151 would require densities  $\geq 10^{8.5} \text{ cm}^{-3}$  (Bromage et al. 1985). Nevertheless, as often noted (cf. Shields & Hamann

1997), the ionic column densities predicted by photoionization models are not particularly sensitive to density. With this in mind, we have assumed a numerical density of atomic hydrogen of  $1 \times 10^7 \text{ cm}^{-3}$  typical of the inner NLR in Seyfert galaxies (cf. Kraemer et al. 1998a), and located the absorbers in the intermediate zone between the inner NLR and outer BLR, as suggested by Espey et al. (1998). We have assumed solar abundances (cf. Grevesse & Anders 1989) for the UV absorber models, with numerical abundances relative to hydrogen as follows: He=0.1, C= $3.4 \times 10^{-4}$ , O= $6.8 \times 10^{-4}$ , N= $1.2 \times 10^{-4}$ , Ne= $1.1 \times 10^{-4}$ , S= $1.5 \times 10^{-5}$ , Si= $3.1 \times 10^{-5}$ , Mg= $3.3 \times 10^{-5}$ , Fe= $4.0 \times 10^{-5}$ . Cosmic dust was not included.

In order to examine a range of conditions, we varied the ionization parameter for the absorber,  $U_{abs}$ , where:

$$U_{abs} = \int_{\nu_0}^{\infty} \frac{L_{\nu}}{h\nu} d\nu / 4\pi D^2 n_H c, \quad (6)$$

where  $L_{\nu}$  is the frequency dependent luminosity of the ionizing continuum,  $D$  is the distance between the central source and the absorber,  $n_H$  is the density of atomic hydrogen and  $h\nu_0 = 13.6 \text{ eV}$ . Models were generated over the range  $10^{-3.5} \leq U_{abs} \leq 10^{-2}$ . This is quite similar to the range of ionization parameters calculated for those kinematic components detected in GHRS spectra of NGC 4151 for which both C IV and Mg II absorption lines could be identified (Kriss 1998). This range is much lower than the typical values for an X-ray absorber ( $U_{abs} = 0.1 - 10$ , cf. Reynolds & Fabian 1995). Integration was truncated at an effective column density (the sum of the columns densities of ionized and neutral H),  $N_{eff} = 10^{20} \text{ cm}^{-2}$ . This is approximately equal to the sum of the effective column densities from each kinematic component detected in NGC 4151 (Kriss 1998).

## 2.2. Absorber Model Results

The predicted column densities of several ionic species are listed in Table 1. Although there are slight differences in the values predicted for the two different SED’s, the results overall show very similar trends, which is to be expected, since the continua were scaled to produce the same number of ionizing photons. The C IV and Mg II column densities predicted by the models with  $U_{abs} = 10^{-3}$  are a reasonable match for those calculated for the Seyfert 1.5 galaxy NGC 4151 (Weymann et al. 1997; Kriss 1998), although they are larger than any *single* component measured by those authors. We should note that our single component absorber is an idealized model, since a set of absorbers with smaller effective column densities and different radial velocities, distributed along the line-of-sight, would have a similar cumulative effect on the ionizing continuum.

In the most highly ionized cases, where  $U_{abs} = 10^{-2}$ , the models predict C IV columns at least an order of magnitude in excess of that observed for NGC 4151 (Weymann et al 1997). This could be compensated by truncating the models at lower effective column density, but then the predicted Mg II columns are too low. Of course, gas at such a low state of ionization could not produce the observed columns of O VII and O VIII seen in many X-ray absorbers (George et al. 1998a). It is possible, then, that the some of the absorption components are due to traces of C IV and N V in a X-ray absorber with greater effective column density, rather than low ionization, optically thin gas (Mathur et al. 1995).

Although C IV and Mg II absorption can coexist in the low-ionization models, i.e. with  $U_{abs} \leq 10^{-3}$  for both SED’s, we did not obtain large columns of N V absorption together with Mg II. NGC 4151 is the only source in which the presence of absorption by all three of these ionic species has been confirmed (cf. Crenshaw et al. 1998). Unfortunately, the spectral region around N V  $\lambda 1241$  has not been observed at sufficiently high resolution for the identification of individual absorption components with those of C IV  $\lambda 1550$  and

Mg II  $\lambda 2800$ , although the low resolution spectra indicate a large column density for N V ( $\sim 10^{15} \text{ cm}^{-2}$ ), suggesting a strong high ionization component. We predict that the N V columns from those components that show Mg II absorption are likely to be below the detection limits ( $< 10^{13} \text{ cm}^{-2}$ ). This prediction will be tested with upcoming STIS observations of NGC 4151. Thus, is it likely that the N V absorption, and possibly some of the C IV absorption, occurs in the X-ray absorber or in more highly ionized, optically thin UV absorbing gas, both of which will be transparent to the ionizing continuum below a few hundred eV.

These models span a range of UV absorber properties, which also show a range of effects on the EUV continuum. The results are also listed in Table 1, and displayed graphically in Figures 1 and 2, for the power-law and BBB models, respectively. Comparing the ratio of incident ionizing radiation to that which escapes the back-end of the absorber at different energies ( $f_E$  in Table 1), we see that, as expected, first the absorption builds above the He II Lyman limit, then near the hydrogen Lyman limit, and more gradually at energies above 100 eV. In Figures 1 and 2, the absorption edges of He I (24.6 eV), O II (35.1 eV), and C III (47.4 eV) are also clearly visible in the filtered spectrum from the  $U_{abs} = 10^{-3}$  model. There are two important effects resulting from the absorption of the ionizing continuum. First, there is a decrease in the fraction of ionizing radiation reaching the NLR. To get a quantitative measure of this effect, consider a typical narrow line cloud, of density  $n_H = 10^5 \text{ cm}^{-3}$ , with an ionization parameter  $U_{nlr} = 10^{-2.5}$  (although one could use any set of conditions for this comparison). Table 1 also shows the ionization parameter for a cloud of the same density, at the same distance from the ionizing source, if it were screened from the source by the UV absorber. For the most extreme case,  $U_{nlr}$  can be reduced by approximately two orders of magnitude. Therefore, for objects with the same intrinsic SED, the presence of a low ionization UV absorber with large covering factor can cause dramatic differences in the conditions in the NLR, and the resulting emission line spectrum. The

effect will be particularly pronounced for line ratios that are good ionization parameter diagnostics, such as [O III]  $\lambda 5007$ /[O II]  $\lambda 3727$  (cf. Ferland & Netzer 1983).

The second spectral property that these absorber models predict is the absorption of the soft X-ray continuum below 100 eV, primarily by He II. At low spectral resolution (i.e.  $\sim 40\%$ ), such as that provided by the *ROSAT* Position Sensitive Proportional Counter (PSPC), this absorption would be manifested by an apparent flattening of the observed continuum. In Figures 3 and 4 we compare the incident and transmitted continua from 100 eV to 5 keV for the four UV absorber models, as indicated by the value of the ionization parameter. As the He II absorption edge builds, the low energy end of this band of the ionizing continuum becomes increasingly suppressed. Neutral hydrogen is an important source of opacity for the lowest ionization models. We can obtain a quantitative measure of the continuum flattening by calculating the spectral index from 0.1 to 2.4 keV (to match the *ROSAT*/PSPC spectral range),  $\alpha_{soft-Xray}$ , for a linear (i.e. power law) fit to  $\log(F_\nu)$  vs.  $\log(\nu)$ . For the power law models, the unattenuated continuum can be fit with  $\alpha_{soft-Xray} \sim -1.38$ . For comparison, the transmitted continuum for the UV absorber with  $U_{abs} = 10^{-3}$  has an  $\alpha_{soft-Xray} \sim -0.86$ . If the covering factor for the UV absorber is 90%, rather than unity,  $\alpha_{soft-Xray}$  becomes  $-0.97$  for the  $U_{abs} = 10^{-3}$  model. For the BBB models, the results are similar ( $\alpha_{soft-Xray} \sim -2.07$ , unattenuated, and  $-1.58, -1.68$ , for the  $U_{abs} = 10^{-3}$  model, 100% and 90% covering, respectively). It is worthwhile to note that there would be no change to the index calculated from a power-law fit between the non-ionizing UV (energies  $< 13.6$  eV) and the X-ray (energies  $> 2$  keV),  $\alpha_{UV-2keV}$  (see Section 3.2), if the absorber were *dust-free*, such as those modeled in this paper.

To summarize, the presence of a UV absorber with a large covering factor along the line of sight will modify the soft X-ray band of the ionizing continuum. The lower the ionization state of the absorber, the more pronounced the effect, which we have illustrated

by holding the  $N_{eff}$  fixed. Also, if the covering factor of the absorber is large along the line of sight to the NLR, the fraction of ionizing photons reaching the NLR is inversely proportional to the ionization parameter of the absorber. This would have a profound effect on the narrow emission line ratios. However, when viewed in the context of a sample of objects, the effects of the modified SED may be diluted by variations in the physical conditions in the NLR gas among Seyfert galaxies. A third effect of the UV absorber is to change the SED below 100 eV, as indicated by Figures 1 and 2 and the values of  $f_E$  in Table 1. To examine the results of this effect on the conditions in the NLR, we have generated a second set of photoionization models. The predictions of these models are discussed in the following section.

### 2.3. Narrow Line Models

It is well known that the conditions in the Narrow Line Region (NLR) of Seyfert galaxies are affected by processes other than photoionization by the central source, such as starbursts (cf. Heckman et al 1997), collisional effects such as shocks (cf. Allen, Dopita & Tsvetanov 1998) and heating by cosmic rays (Ferland & Mushotzky 1984). Also, line ratios can be affected by the relative contribution from matter-bounded gas (Binette, Wilson & Storchi-Bergmann 1996). Nevertheless, it is likely that photoionization is the dominant mechanism for ionization and heating in the NLR, as Ferland has argued (cf. Ferland & Netzer 1983). This is supported by detailed models of individual objects (cf. Kraemer et al. 1998a), which also show that the composite emission-line spectrum appears to be dominated by radiation-bounded gas. Furthermore, the NLR models that we present are intended to examine the effects of modification of the SED by an intervening absorber, and therefore we are foremost concerned with photoionized gas. The interpretation of observational evidence for this effect, however, requires us to address some of these concerns, which we will do in

the Discussion section.

The predicted emission line ratios from the photoionization models of typical NLR clouds are listed in Tables 2 and 3 (for comparison to the NLR spectra of Seyfert 1.5s, see Cohen (1983)). For each intrinsic SED, NLR models of gas of density  $n_H = 10^5 \text{ cm}^{-3}$  and solar abundances (see section 2.1) were generated for the case of an unattenuated source, and both 100% and 90% covering by each of the four different UV absorber models. The models were truncated at an  $N_{eff} = 10^{21} \text{ cm}^{-2}$ , which we have found to be a reasonable average for a mix of radiation- and matter-bounded gas in the NLR of Seyferts (cf. Kraemer et al. 1998a). Since we are primarily interested in the gross effect of the SED on the physical conditions in the NLR, only a subset of the emission-line ratios predicted by the models are listed. In order to make the comparison of the NLR model predictions simpler, we held the ionization parameter for the NLR cloud fixed at  $U_{nlr} = 10^{-2.5}$ . Holding  $U$  fixed required scaling up the flux as the UV absorbers screen out more of the ionizing radiation. This was done by decreasing the distance between the NLR cloud and the ionizing source. The absorption of the continuum was so extreme for model 4 that the scaling became unrealistic, effectively placing the NLR cloud *closer* to the ionizing source than the absorber. Each model predicted the same average  $H\beta$  emissivity (with the exception of the power-law SED Model 4, which had a slightly lower emissivity due to the higher fractional ionization of hydrogen).

The narrow He II  $\lambda 4686/H\beta$  ratio is quite sensitive to the shape of the ionizing continuum, since neutral hydrogen is the dominant source of opacity near 13.6 eV, while ionized helium is above 54.4 eV. Comparing the model predictions for this ratio provides us with the most direct way to see the effect of the different SED's. He II  $\lambda 4686/H\beta$  for the unattenuated case is 0.21 and 0.25 for the power-law and BBB models, respectively, which is approximately the value expected from a photon counting calculation (cf. Kraemer &

Harrington 1986). As the ionization parameter of the absorber decreases, we start to see the expected effect on this line ratio, with the value dropping to 0.07 for Model 2 for the case of full source coverage by the UV absorber. Then, as the attenuation of the continuum becomes more extreme, the He II  $\lambda 4686/\text{H}\beta$  ratio begins to increase up to three times the value predicted by the unattenuated model for the most absorbed continuum. Although this is partially an artifact of the scaling used to fix the ionization parameter of the NLR models, there is also a reflection of the physical conditions in X-ray ionized gas. In the most extreme case, i.e. Model 4, the modified ionizing continua includes a significant remnant of photons near 100 eV, where He I and He II cross-sections dominate, but effectively no photons at the Lyman limit, resulting in an unusual mix of low and high ionization species. Finally, as expected, the inclusion of a fraction (10%) of unattenuated continuum mitigates these effects, although not to the point where they would be undetectable.

Due to the choice of ionization parameter, the high ionization collisional lines are weak in these models, and we have only listed ratios for C IV  $\lambda 1550$ , [Ne IV]  $\lambda 2423$  and [Ne V]  $\lambda 3426$  in Tables 3 and 4. A similar effect is seen for these lines as for He II  $\lambda 4686$ , and the two neon lines track the He II line most closely, as one would expect since the ionization potentials of their parent ionic states are above 54.4 eV. Lines from intermediate ionization states with parent ionization potentials well below 54.4 eV, including [O III]  $\lambda 5007$ , [O III]  $\lambda 4363$ , [O II]  $\lambda 3727$ , [N II]  $\lambda\lambda 6548, 6584$ , and [Ne III]  $\lambda 3869$ , show little variation in relative strength until the X-ray component of the ionizing continuum dominates, i.e. in Models 3 and 4. The low ionization lines such as [O I]  $\lambda 6300$  and Mg II  $\lambda 2800$  also show the effects of the increased hardness of the attenuated continua, although the scaling of model 4 continuum causes an increase in the ionization fraction that suppresses the Mg II line somewhat. The oxygen is tightly bound to the neutral fraction of hydrogen by charge exchange, so the scaling effect is not obvious when looking at oxygen line ratios relative to  $\text{H}\beta$ .

The Balmer decrement is strongly affected by collisional excitation in X-ray heated gas, as noted by Netzer (1982) and Gaskell & Ferland (1984), and this is clearly seen in this set of models. Also,  $\text{Ly}\alpha/\text{H}\beta$  increases as the ionizing continuum becomes harder, as expected. It should be noted that very large values of  $\text{H}\alpha/\text{H}\beta$  and  $\text{Ly}\alpha/\text{H}\beta$  are predicted for the most extreme cases (Model 4). Although this fits an extrapolation of the results presented in Gaskell and Ferland, the code has not been compared in detail with other models for this extreme case, and, as such, the predictions for these two ratios should be taken qualitatively.

The differences between the power-law models and corresponding BBB models are subtle. In the BBB models a larger residual of photons remains below 100 eV after attenuation by the UV absorber, so the effects on the NLR gas are less pronounced. Observationally, it would be hard to distinguish between the two intrinsic SED's on the basis of narrow line ratios, except, perhaps, from the relative strength of the [O I] lines, but these lines depend on the optical depth of the emission line clouds, which is almost certain to vary among objects.

#### 2.4. Summary of Modeling Results

From the set of photoionization models described in the previous sections, we have been able to show that a UV absorber that possesses observable columns for a range of ionic species, including Mg II, will attenuate the ionizing continuum in such a way that the conditions in the NLR will be affected (assuming a large covering factor). Even when holding the ionization parameter fixed for the NLR models, the predicted line ratios show the gross effects of the continuum attenuation which should be observable. If we had allowed the ionization parameter to vary, as the values for  $U_{nlr}$  in Table 1 show, the effect on the NLR models would have been even more dramatic.

The following set of conditions may exist in individual objects:

1. If intrinsic UV resonance line absorption is present, the continuum along the line of sight will be attenuated, near the He II Lyman limit for a more highly ionized absorber, then near the hydrogen Lyman limit and finally at soft X-ray energies as the absorber becomes more neutral. Although most of the EUV waveband is unobservable, *ROSAT* and *ASCA* observations in the soft X-ray (0.1 to 2 keV) should show the effects of attenuation by a UV absorber, particularly if its presence is flagged by Mg II absorption.
2. If the covering factor of the absorber is large, its effect on the conditions in the NLR gas will be observable, particularly in the line ratios most sensitive to the SED such as He II  $\lambda 4686/\text{H}\beta$ .
3. Unless the absorber is dusty or Compton thick ( $> 10^{24}\text{cm}^{-2}$ ) there will not be any effect on the continuum below the Lyman limit. If the attenuation of the X-ray continuum above 2 keV is relatively small, the optical to X-ray index,  $\alpha_{UV-2keV}$ , will not be correlated with these other observables (although determination of the 2 keV flux depends on accurate modeling of the low energy X-ray spectrum, and therefore can be biased by an improper correction for absorption).

In the following sections we will discuss the observational evidence for these conditions.

These models also predict that the total emission from the UV absorbing gas could be comparable to that from the NLR gas, assuming that the covering factors are similar. This, of course, depends on the density and/or location of the absorber. Nevertheless, the presence of this emission in the narrow-line spectrum will dilute some of the effects of the modified ionizing continuum. The predicted emission line ratios from the absorber models are listed in Tables 4 and 5. In the higher ionization cases, the UV absorber could be a source of emission from coronal lines such as [Ne V]  $\lambda 3426$  and [Fe VII]  $\lambda 6087$ .

Interestingly, the conditions for our high ionization parameter models are similar to those used in modeling the NLR of NGC 5548 (Kraemer et al. 1998a), which suggests that some of the C IV absorption in NGC 5548 might arise in NLR gas. It is also possible that strong semi-forbidden lines, such as C III]  $\lambda$ 1909 and C II]  $\lambda$ 2326 emission may arise in this gas, even in the lower ionization cases.

### 3. Comparison with Observations

In order to compare our model results to the observations most effectively, we have chosen to concentrate on Seyfert 1.5s (for the sake of simplicity, we will refer to all intermediate Seyfert galaxies as type 1.5s). The presence of X-ray and UV intrinsic absorption has been detected in both Seyfert 1s and Seyfert 1.5s, and for each subclass the fact that we observe emission from the BLR is evidence that we are seeing the AGN directly. However, in Seyfert 1.5 spectra it is possible to separate out the narrow emission-line component much more easily than for Seyfert 1s. Seyfert 2s are unsuitable since the ionizing source is generally obscured (cf. Antonucci 1994) and only a scattered component of the BLR emission and soft X-ray continuum can be observed, and the latter may be contaminated by a starburst (Turner et al. 1997).

We selected a set of Seyfert 1.5 galaxies for which narrow He II  $\lambda$ 4686/H $\beta$  ratios had been measured. The sample includes the 13 Seyfert 1.5s studied by Cohen (1983), which is the largest set thereof, NGC 4151 (cf. Ferland and Mushotzky 1982), NGC 3516 (Ulrich & Pequignot 1980), and LB 1727 (Turner et al. 1998). For this set, the values of narrow He II  $\lambda$ 4686/H $\beta$  range from 0.14 to 0.43, with an average close to the values assumed for our unattenuated NLR models.

### 3.1. Narrow Emission Lines

A detailed comparison of the observed narrow emission-line ratios of each of the Seyfert 1.5s in our sample to our model predictions is outside the scope of this paper (see Kraemer et al. 1998a for an example of this type of analysis). However, Kraemer et al. (1998b) examined several selected line ratios for this set of objects, from which we can make a qualitative assessment of the model predictions. First, the relative [O I] strength is weakly anti-correlated with the He II strength, as predicted (with a correlation coefficient,  $r_s = -0.44$  and a probability,  $P_r = 0.12$ , of exceeded  $r_s$  in a random sample). Second, there is a strong correlation of [O III]  $\lambda 5007$ /[O II]  $\lambda 3727$  vs. He II  $\lambda 4686$ /H $\beta$  ( $r_s = 0.76$ ,  $P_r = 0.002$ ), similar to a trend that has been noted for the [O III]  $\lambda 5007$  vs. He II  $\lambda 4686$  (Cohen 1983). Although this could be explained by the contribution from highly ionized, matter-bounded gas, as in the case examined by Binette et al. (1996), it also fits with the predictions for an attenuated ionizing continuum.

### 3.2. The Soft X-ray Continuum and He II $\lambda 4686$ /H $\beta$

In Seyfert galaxies, the hard X-ray spectrum above 2 keV can be characterized by a fairly flat power law, with a typical index,  $-1.0 \lesssim \alpha \lesssim -0.5$  (e.g., Nandra & Pounds 1994). In the soft X-ray band ( $\lesssim 1$  keV) attenuation by neutral and/or ionized material along the line-of-sight becomes important (e.g., George et al. 1998a and references therein). The flattest X-ray (2-10 keV) spectra have been observed in Seyfert 1.5 galaxies (e.g., NGC 4151, Weaver et al. 1994; NGC 3227, George et al. 1998b) and in most known cases at least part of the nuclear continuum is heavily absorbed, although the connection between absorption and index has not been fully explored.

Many Seyfert spectra appear to steepen below  $\sim 1$  keV (e.g. Arnaud et al. 1985,

Turner & Pounds 1989, Turner et al. 1998). The luminosities and variability seen in the soft X-ray regime suggests these “soft X-ray excesses” are often dominated by an upturn in the underlying continuum, and the strength of the soft component for Seyfert 1s varies but the slope appears to be well-correlated with the ratio of the UV flux at 1375Å to the flux at 2 keV (Walter & Fink 1993). In at least some sources, this soft X-ray component may be a power-law which extends to join the UV continuum (e.g. Nandra et al. 1995, Zheng et al. 1997, Laor et al. 1997); in this case there should be a correlation between EUV-dependent line ratios and the soft X-ray index.

The soft X-ray indices for each of the Seyfert 1.5s in our sample are listed in Table 6, and were determined by fits to an absorbed power-law model. Most indices were measured from *ROSAT*/PSPC data (from 0.1 - 2.4 keV). NGC 3227 and Mrk 6 were derived from fits to the *ASCA* data (George et al. 1998b, Feldmeier et al. 1998, respectively) which gives a more accurate index as *ASCA* allows a better modeling of the complex absorption. In the case of MCG 8-11-11 the lack of a pointed PSPC observation led us to use the 0.7 - 10 keV index from the *Einstein* Solid State Spectrometer/Monitor Proportional Counter (Turner et al. 1991).

From these results, there appears to be a modest anti-correlation between X-ray hardness and the He II  $\lambda 4686/\text{H}\beta$  ratio ( $r_s = -0.47$ ,  $P_r = 0.08$ ), in the sense that sources with steep soft X-ray spectra, show relatively strong He II, as shown in Figure 5. However, given the small number of data points, care should be taken in interpreting this trend. A more conservative interpretation is that there is a zone of exclusion, specifically the intersection of flat soft X-ray slope and large He II  $\lambda 4686/\text{H}\beta$ . As we have shown, the presence of absorbing material, residing between the X-ray emitting region and the NLR could explain this anti-correlation. In fact, the measured soft X-ray indices for the flatter sources (specifically NGC 4151, NGC 3227, Mrk 6, and MCG 8-11-11) are similar to those

predicted by our UV absorber models. If we are truly seeing the results of attenuation, the implication is that the covering factor is large enough that the NLR is exposed to the same continuum as observed in the soft X-ray band.

In Table 6, we also list the UV to X-ray indices,  $\alpha_{UV-2keV}$  for those objects for which data were available. As noted, they were either calculated from the values listed in Walter & Fink (1993) or from the UV fluxes at 1460Å in the *IUE* low dispersion archive and the 2 keV luminosity densities determined from *Einstein* IPC data by Wilkes et al (1994), assuming an intrinsic X-ray index of  $-1.0$ . Although for the most part the  $\alpha_{UV-2keV}$  and  $\alpha_{soft-Xray}$  are similar, there are several cases, once again those sources with the flattest soft X-ray slopes, where they disagree. If, as Walter & Fink's (1993) assert, the shape of the UV to soft X-ray bump does not vary among Seyfert 1 galaxies, this result may be interpreted as evidence that  $\alpha_{UV-2keV}$  and  $\alpha_{soft-Xray}$  match when the intrinsic continuum is observed, while mismatches are the result of attenuation, as our models predict.

### 3.3. Intrinsic Absorption

As we have seen, there appears to be some correlation between line ratios and the shape of the soft X-ray continuum that qualitatively fit our model predictions. A better test of the models is associating these properties with the intrinsic UV absorption.

Among the Seyfert 1.5 galaxies, those with the flattest soft X-ray spectra, (specifically NGC 4151, NGC 3227, and MCG 8-11-11) are known to have unusually strong intrinsic absorption. *IUE* and *HST* spectra of NGC 4151 reveal high column densities for lines covering a wide range in ionization (Mg II to N V, see Weymann et al. 1997), and the presence of absorption by metastable C III\*  $\lambda 1175$  ((note also that Balmer and He I self absorption are seen in the optical (cf. Anderson & Kraft 1969); we have not attempted to

model the conditions that would produce these features). *IUE* spectra of NGC 3227 and MCG 8-11-11 also appear to show the presence of large absorption columns (Ulrich 1988). Kriss et al. (1997) report a possible Lyman limit detection in *HUT* spectra of NGC 3227. These objects all appear to have a mismatch of  $\alpha_{soft-Xray}$  and  $\alpha_{UV-2keV}$ , which, as noted above, is what might be expected for a continuum modified by a UV absorber. The galaxies with low ionization absorption can be contrasted with that of objects like NGC 5548 and NGC 7469, which show absorption by C IV and N V, but not Si IV or Mg II. The  $\alpha_{soft-Xray}$  and  $\alpha_{UV-2keV}$  are quite similar in these objects, which is agreement with the results from our more highly ionized UV absorber models.

If we include emission line ratios, the overall picture becomes more complicated. Although most of those with flatter soft X-ray spectra are weak He II emitters, NGC 3227 is an exception. This can be interpreted as indicating that the unattenuated ionizing continuum is unusually hard, the NLR gas is matter-bounded, or that the covering factor of the UV/soft X-ray absorber is low, except along our line of sight. However, our models predict that in the case of a very low ionization UV absorber the narrow He II  $\lambda/H\beta$  can be larger in shielded gas than in gas that is directly exposed to the ionizing source. Also, as the ionization state of the absorber decreases, the [O I]  $\lambda 6300/H\beta$  ratio will increase. The narrow line spectrum of NGC 3227 shows strong [O I] emission (0.8 x  $H\beta$ , (Cohen 1983)), which indicates that the NLR gas is radiation-bounded and suggests that the ionization state of the UV absorber may be particularly low. It will require *HST/STIS* observations to test this prediction.

The case of NGC 7469 also merits an explanation. This object, which shows the presence of a high ionization state UV absorber (Crenshaw et al. 1998), has both weak He II and a steep soft X-ray slope, one that matches the  $\alpha_{UV-2keV}$  quite closely. In fact, the He II is weaker than a simple photon counting calculation would predict. It is known,

however, that a starburst is present in NGC 7469 (cf. Wilson et al. 1991). We would suggest that the starburst is diluting the relative He II strength, and that He II  $\lambda 4686/\text{H}\beta$  in the AGN ionized gas is probably similar to NGC 5548.

As we have noted several times, our analysis of the effect of the modified ionizing continuum on the NLR gas is based on the assumption that the covering factor of the low ionization absorber is large (i.e.  $> 0.5$ ). Although there are a large fraction of Seyfert 1s that show intrinsic UV absorption (Crenshaw et al. 1998), which implies a large covering factor, there is no a priori reason to assume that the low ionization absorber is associated with the high ionization UV absorber (or the X-ray absorber). Another possibility is that the low ionization absorption lines are formed in an atmosphere above the molecular torus, the existence of which is a fundamental prediction of the “unified” model for Seyfert galaxies (cf. Antonucci 1994). Kriss et al. (1997) suggest that in several cases (NGC 4151, NGC 3516, and NGC 3227), our line of sight to the BLR is through this atmosphere, along the plane of the torus. From this viewing angle, the biconical distribution of the emission line gas should be quite evident. This is certainly true for NGC 4151, but less clear for the other cases (cf. Schmitt & Kinney 1996). Also, if this model is correct, we should still see an absorbed soft X-ray continuum when low ionization absorption is present. The fact that a large fraction of Seyfert 1.5s have a flat soft X-ray slope appears to support association of the low ionization gas with the high ionization intrinsic absorption, a point to which we will return in the Discussion section.

#### 4. Discussion

Our basic model predicts that a UV absorber, situated between the BLR and NLR and with a large covering factor, will have an observable effect on the soft X-ray continuum and narrow emission-line spectrum. We have generated a set of model UV absorbers, spanning a

range of ionization parameter. The predicted ionic columns densities, except in the highest ionization models, are a reasonable match to those observed in the most heavily obscured Seyfert 1.5 galaxies. We have also demonstrated the effects of attenuation by this gas on conditions in the NLR, both by calculating the ionization parameters for a “typical” NLR cloud shielded by these absorbers and by generating a set of NLR models at fixed ionization parameter. Also, we have shown that significant soft X-ray attenuation by this absorbing layer can result in an apparent flattening soft x-ray spectrum (when observed at low spectral resolution), as shown in Figures 3 and 4. Finally, there are sources where the full set of predicted characteristics are present. If this model is correct, we should be able to predict the presence of one characteristic, such as UV absorption, if the other two are observed: a low ionization, He II weak narrow-line spectrum and a flat soft X-ray spectrum.

As noted above, the spectral characteristics of NGC 4151 match the model predictions quite well, and MCG 8-11-11 and NGC 3227 also show evidence that the same process is at work. Specifically, we predict that more than 1/3 of the Seyfert 1.5s in our sample (specifically those with  $\alpha_{soft-Xray} \leq -1.0$ ; see Table 6) possess a large column of low ionization UV absorption. If, as Kriss et al. (1997) suggest, the low ionization lines form in an atmosphere associated with the molecular torus, either the atmosphere must extend well above the plane of the torus or the characteristics of Seyfert 1.5s, e.g. the detection of a narrow component in the permitted emission lines, are more easily observed when the AGN is viewed along this line-of-sight. If the former were true, the covering factor of the absorber along the line of sight to the NLR could still be large, and our predictions on the effect in the NLR gas are relevant.

## 5. Summary

We have explored the effect of the gas in which intrinsic UV absorption lines arise on the ionizing continuum in Seyfert galaxies. The main results are the following:

1. Above 100 eV, the absorber will modify the soft X-ray continuum, if the column density is sufficiently large ( $N_{eff} \geq 10^{20} \text{ cm}^{-2}$ ) and the gas is not highly ionized ( $U_{abs} \leq 10^{-2.5}$ ), as is the case for NGC 4151. There is observational evidence for this effect, since objects that show large columns of low ionization absorbers tend to have flatter soft X-ray continuum slopes.
2. A low ionization absorber will attenuate much of the ionizing radiation between 13.6 eV and 100 eV, in particular near the He II Lyman limit. There is evidence for this in that the relative strength of the narrow He II line is anti-correlated with the hardness of the soft X-ray continuum in Seyfert 1.5s.
3. Since the presence of low ionization UV absorption and a flat soft X-ray continuum may be interrelated, one can predict that a Seyfert galaxy will exhibit one of these characteristics if the other is present. If so, a large fraction (1/3) of Seyfert 1.5s should show low ionization UV absorption lines. Also, if the covering factor of the low ionization gas is close to unity, we would expect that these absorbed Seyfert 1.5s will possess low ionization narrow emission-line spectra.

S.B.K. thanks Eric Smith for useful discussions. S.B.K. and D.M.C. acknowledge support from NASA grant NAG5-4103. T.J.T. acknowledges support from UMBC and NASA/LTSA grant NAG5-7835.

## REFERENCES

Allen, M.G., Dopita, M.A., & Tsevtanov, Z.I. 1998, *ApJ*, 493, 571

Anderson, K.S., & Kraft, R.P. 1969, *ApJ*, 158, 859

Antonucci, R.R. 1994, *ARA&A*, 31, 64

Arnaud, K.A. et al. 1985, *MNRAS*, 217, 105

Baldwin, J.A. 1977, *ApJ*, 214, 679

Binette, L., Wilson, A.S., & Storchi-Bergmann, T. 1996, *A&A*, 312, 365

Bromage, G.E., et al. 1985, *MNRAS*, 215, 1

Cohen, R.D. 1983, *ApJ*, 273, 489

Crenshaw, D.M. et al. 1998, *ApJ*, in press.

Espey, B.R., et al. 1998, *ApJ Letters*, in press

Ferland, G.J., & Mushotzky, R.F. 1982, *ApJ*, 262, 564

Ferland, G.J., & Netzer, H. 1983, *ApJ*, 264, 105

Ferland, G.J., & Mushotzky, R.F. 1984, *ApJ*, 286, 42

Feldmeier, J.J., et al. 1998, *ApJ*, in press

Gaskell, C.M., & Ferland, G.J. 1984, *PASP*, 96, 393

George, I.M. et al., 1998a, *ApJS*, 114, 73

George, I.M. et al., 1998b, *ApJ*, in press

Grevesse, N., & Anders, E. 1989, in *Cosmic Abundances of Matter*, ed. C.J. Waddington (New York: AIP), 1

Heckman, T.M., et al. 1997, *ApJ*, 482, 114

Korista, K.T., Ferland, G.J., & Baldwin, J.A. 1997, *ApJ*, 487, 555

Kraemer, S.B. 1985, Ph.D. thesis, Univ. Maryland

Kraemer, S.B., & Harrington, J.P. 1986, ApJ, 307, 478

Kraemer, S.B., Wu, C.-C., Crenshaw, D.M., & Harrington, J.P. 1994, ApJ, 435, 171

Kraemer, S.B., Crenshaw, D.M., Filippenko, A.V. & Peterson, B.M. 1998a, ApJ, 499, 719

Kraemer, S.B., Crenshaw, D.M., Turner, T.J., & George, I.M. 1998b, in Structure and Kinematics of Quasar Broad Line Regions, ed. C.M. Gaskell, W.N. Brandt, M. Dietrich, D. Dultzin-Hacyan, & M. Eracleous (San Francisco: Astronomical Society of the Pacific), ASP Conference Series, in press

Kriss, G.A.. et al. 1997, in Emission Lines in Active Galaxies: New Methods and Techniques, ed. B.M. Peterson, F.-Z. Cheng, & A.S. Wilson (San Francisco: Astronomical Society of the Pacific), ASP Conference Series, 113, 453

Kriss, G.A. 1998, in The Scientific Impact of the Goddard High Resolution Spectrograph, ed. J.C. Brandt, T.B. Ake, & C.C. Petersen (San Francisco: Astronomical Society of the Pacific), ASP Conference Series, 143, 271

Laor, A., et al. 1997, ApJ, 477, 93

Malkan, M.A. 1983, ApJ, 268, 582

Mathews, W.G., & Ferland, G.J. 1987, ApJ, 323, 456

Mathur, S., Elvis, M. & Wilkes, B. 1995, ApJ, 452, 230

Nandra, K., & Pounds, K.A. 1994, MNRAS, 268, 405

Nandra, K., et al. 1995, MNRAS, 273, 85

Netzer, H. 1982, MNRAS, 198, 589

Reynolds, C.S., & Fabian, A.C. 1995, MNRAS, 273, 1167

Reynolds, C.S. 1997, MNRAS, 286, 513

Rush, B., Malkan, M.A., Fink, H.H., & Voges, W. 1996, *ApJ*, 471, 190

Schmitt, H.R., & Kinney, A.L. 1996, *ApJ*, 463, 498

Shields, J.C., & Hamann, F. 1997, *ApJ*, 481, 752

Shull, J.M., & Sachs, E.R. 1993, *ApJ*, 416, 536

Turner, T.J., & Pounds, K.A. 1989, *MNRAS*, 240, 833

Turner, T.J. et al. 1991, *ApJ*, 381, 85

Turner, T.J., George, I.M., Nandra, K., & Mushotzky, R.F. 1997, *ApJS*, 113, 23

Turner, T.J. et al. 1998, *ApJ*, submitted

Ulrich, M.-H., Pequignot, D. 1980, *ApJ*, 238, 45

Ulrich, M.-H. 1988, *MNRAS*, 230 121

Voit, G.M., Shull, J.M., & Begelman, C. 1987, *ApJ*, 316, 573

Walter, R., & Fink, H.H. 1993, *A&A*, 274, 105

Weaver, K.A., et al. 1994, *ApJ*, 436, L27

Weymann, R.J., et al. 1997, *ApJ*, 483, 717

Wilkes, B.J., et al. 1994, *ApJS*, 92, 53

Wilson, A.S., Helfer J.T., Haniff, C.A., & Ward, M.J. 1991, *ApJ*, 381, 79

Zheng, W., et al. 1995, *ApJ*, 444, 632

Zheng, W., et al. 1997, *ApJ*, 475, 469

Fig. 1.— Spectral Energy Distribution, 8.7 eV – 100 eV, for the power law models; the solid line represents the incident continuum and the dashed line the filtered continuum, for the  $U = 0.01$  and  $0.001$  models,  $N_{eff} = 10^{20} \text{ cm}^{-2}$ . The energies of several absorption edges are noted.

Fig. 2.— Spectral Energy Distribution, 8.7 eV – 100 eV, for the BBB models; the solid line represents the incident continuum and the dashed line the filtered continuum, for the  $U = 0.01$  and  $0.001$  models,  $N_{eff} = 10^{20} \text{ cm}^{-2}$ . The energies of several absorption edges are noted.

Fig. 3.— Spectral Energy Distribution, 100 eV – 5 keV, for the power law models; the solid line represents the incident continuum and the dashed line the filtered continuum, for each of the four models ( $N_{eff} = 10^{20} \text{ cm}^{-2}$  in all cases).

Fig. 4.— Spectral Energy Distribution, 100 eV – 5 keV, for the BBB models; the solid line represents the incident continuum and the dashed line the filtered continuum, for each of the four models ( $N_{eff} = 10^{20} \text{ cm}^{-2}$  in all cases).

Fig. 5.— Soft X-ray Index (from a power-law fit, from 0.1 - 2.4 keV, except as noted in text) versus narrow He II  $\lambda/\text{H}\beta$  in the sample of Seyfert 1.5s; error in  $\text{He II}/\text{H}\beta \approx 25\%$ .

Table 4. Emission Line Ratios (relative to  $\text{H}\beta$ ) for UV Absorber Models<sup>a</sup>, assuming a Power-law Ionizing Continuum

	$U_{abs} = 10^{-2.0}$	$U_{abs} = 10^{-2.5}$	$U_{abs} = 10^{-3.0}$	$U_{abs} = 10^{-3.5}$
Ly $\alpha$ $\lambda 1216$	37.27	38.14	40.34	50.36
N V $\lambda 1240$	1.21	0.07	0.00	0.00
Si IV $\lambda 1398$	0.85	1.68	0.13	0.00
O IV] $\lambda 1400$	4.18	0.95	0.04	0.00
N IV] $\lambda 1485$	1.75	0.41	0.03	0.00
C IV $\lambda 1550$	31.31	10.11	0.67	0.03
O III] $\lambda 1664$	1.31	2.65	1.08	0.21
N III] $\lambda 1750$	1.47	1.75	0.63	0.11
C III] $\lambda 1909$	11.23	17.07	7.28	2.21
C II] $\lambda 2326$	0.10	0.92	3.23	4.91
Mg II $\lambda 2800$	0.00	0.30	3.15	4.91
[Ne V] $\lambda 3426$	2.05	0.48	0.01	0.00
[Fe VII] $\lambda 3586$	0.30	0.06	0.00	0.00
[Fe VII] $\lambda 3760$	0.41	0.08	0.00	0.00
[Ne III] $\lambda 3869$	0.08	0.97	1.44	1.17
[O III] $\lambda 4363$	0.95	2.21	1.13	0.26
He II $\lambda 4686$	1.01	0.66	0.23	0.16
H $\beta$	1.00	1.00	1.00	1.00
[O III] $\lambda 5007$	1.06	3.04	2.11	0.61
[Fe VII] $\lambda 5721$	0.42	0.10	0.00	0.00
[Fe VII] $\lambda 6087$	0.63	0.14	0.00	0.00
[O I] $\lambda 6300$	0.00	0.00	0.00	0.50
H $\alpha$ $\lambda 6563$	2.83	2.89	2.96	3.17

<sup>a</sup> $n_H = 1 \times 10^7 \text{ cm}^{-3}$ , no dust,  $N_{eff} = 10^{20} \text{ cm}^{-2}$

Table 5. Emission Line Ratios (relative to  $\text{H}\beta$ ) from UV Absorber Models<sup>a</sup>, assuming a BBB Ionizing Continuum

	$U_{abs} = 10^{-2.0}$	$U_{abs} = 10^{-2.5}$	$U_{abs} = 10^{-3.0}$	$U_{abs} = 10^{-3.5}$
$\text{Ly}\alpha \lambda 1216$	37.24	38.16	41.35	52.50
$\text{N V } \lambda 1240$	1.24	0.07	0.00	0.00
$\text{Si IV } \lambda 1398$	1.65	1.99	0.17	0.00
$\text{O IV] } \lambda 1400$	3.85	1.11	0.06	0.00
$\text{N IV] } \lambda 1485$	1.74	0.50	0.04	0.00
$\text{C IV } \lambda 1550$	29.45	12.34	1.06	0.05
$\text{O III] } \lambda 1664$	0.89	2.22	1.25	0.27
$\text{N III] } \lambda 1750$	1.03	1.50	0.72	0.14
$\text{C III] } \lambda 1909$	7.38	14.82	8.31	2.71
$\text{C II] } \lambda 2326$	0.07	0.67	2.82	4.86
$\text{Mg II } \lambda 2800$	0.00	0.28	3.06	4.92
$[\text{Ne V}] \lambda 3426$	2.09	0.43	0.01	0.00
$[\text{Fe VII}] \lambda 3586$	0.29	0.05	0.00	0.00
$[\text{Fe VII}] \lambda 3760$	0.40	0.06	0.00	0.00
$[\text{Ne III}] \lambda 3869$	0.08	0.84	1.51	1.26
$[\text{O III}] \lambda 4363$	0.65	1.87	1.28	0.32
$\text{He II } \lambda 4686$	1.03	0.78	0.29	0.20
$\text{H}\beta$	1.00	1.00	1.00	1.00
$[\text{O III}] \lambda 5007$	0.71	2.61	2.33	0.61
$[\text{Fe VII}] \lambda 5721$	0.41	0.07	0.00	0.00
$[\text{Fe VII}] \lambda 6087$	0.62	0.10	0.00	0.00
$[\text{O I}] \lambda 6300$	0.00	0.00	0.00	0.45
$\text{H}\alpha \lambda 6563$	2.83	2.89	3.00	3.23

<sup>a</sup> $n_H = 1 \times 10^7 \text{ cm}^{-3}$ , no dust,  $N_{eff} = 10^{20} \text{ cm}^{-2}$

Table 6. Seyfert 1.5s: Soft X-ray Indices

name	narrow He II $\lambda 4686/\text{H}\beta^a$	$\alpha_{soft-Xray}^b$	$\alpha_{UV-2keV}$
NGC 3227	$0.23 \pm 0.07$	$-0.60^c \pm 0.02$	$-1.21^k$
NGC 3516	$0.35 \pm 0.10$	$-1.44^d \pm 0.20$	$-1.58^k$
NGC 4151	$0.19 \pm 0.06$	$-1.06^d \pm 0.24$	$-1.64^k$
NGC 5548	$0.23 \pm 0.05$	$-1.32^d \pm 0.05$	$-1.27^l$
NGC 7469	$0.14 \pm 0.04$	$-1.50^f \pm 0.08$	$-1.52^l$
Mrk 6	$0.15 \pm 0.04$	$-0.46^e \pm 0.87$	
Mrk 79	$0.25 \pm 0.07$	$-1.18^d \pm 0.10$	$-1.30^l$
Mrk 279	$0.16 \pm 0.05$	$-1.32^g \pm 0.03$	$-1.36^l$
Mrk 506	$0.21 \pm 0.06$	$-1.46^h \pm 0.20$	$-1.32^l$
Mrk 704	$0.43 \pm 0.12$	$-1.45^h \pm 0.13$	$-1.36^l$
Mrk 817	$0.29 \pm 0.08$	$-1.90^d \pm 0.24$	
Mrk 841	$0.32 \pm 0.09$	$-1.41^i \pm 0.14$	$-1.70^l$
Mrk 926	$0.14 \pm 0.04$	$-1.00^h \pm 0.31$	$-1.35^l$
MCG 8-11-11	$0.16 \pm 0.05$	$-0.59^j \pm 0.14$	$-0.95^l$
LB 1727	$0.28 \pm 0.06$	$-2.2^f \pm 0.08$	

<sup>a</sup>errors as quoted by Cohen (1983).

<sup>b</sup>see text (Section 3.2) for the description of the derivation of  $\alpha_{soft-Xray}$ .

<sup>c</sup>ASCA (George et al. 1998b).

<sup>d</sup>ROSAT/PSPC (Rush et al. 1996, see text).

<sup>e</sup>ASCA (Feldmeier et al. 1998).

<sup>f</sup>ROSAT/PSPC (Turner, George & Mushotzky 1993).

<sup>g</sup>ROSAT/PSPC (this paper).

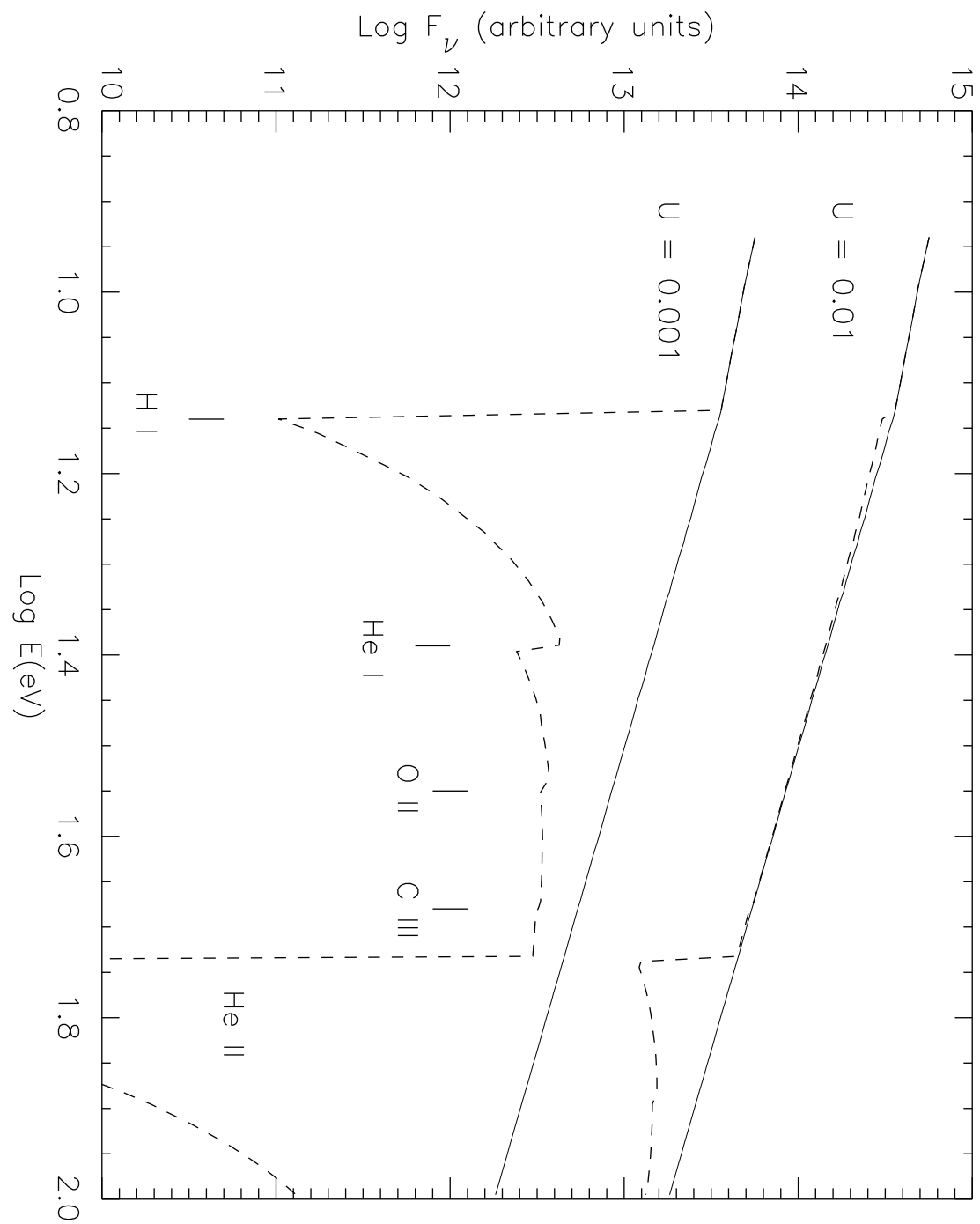
<sup>h</sup>ROSAT/PSPC (Walter & Fink 1993).

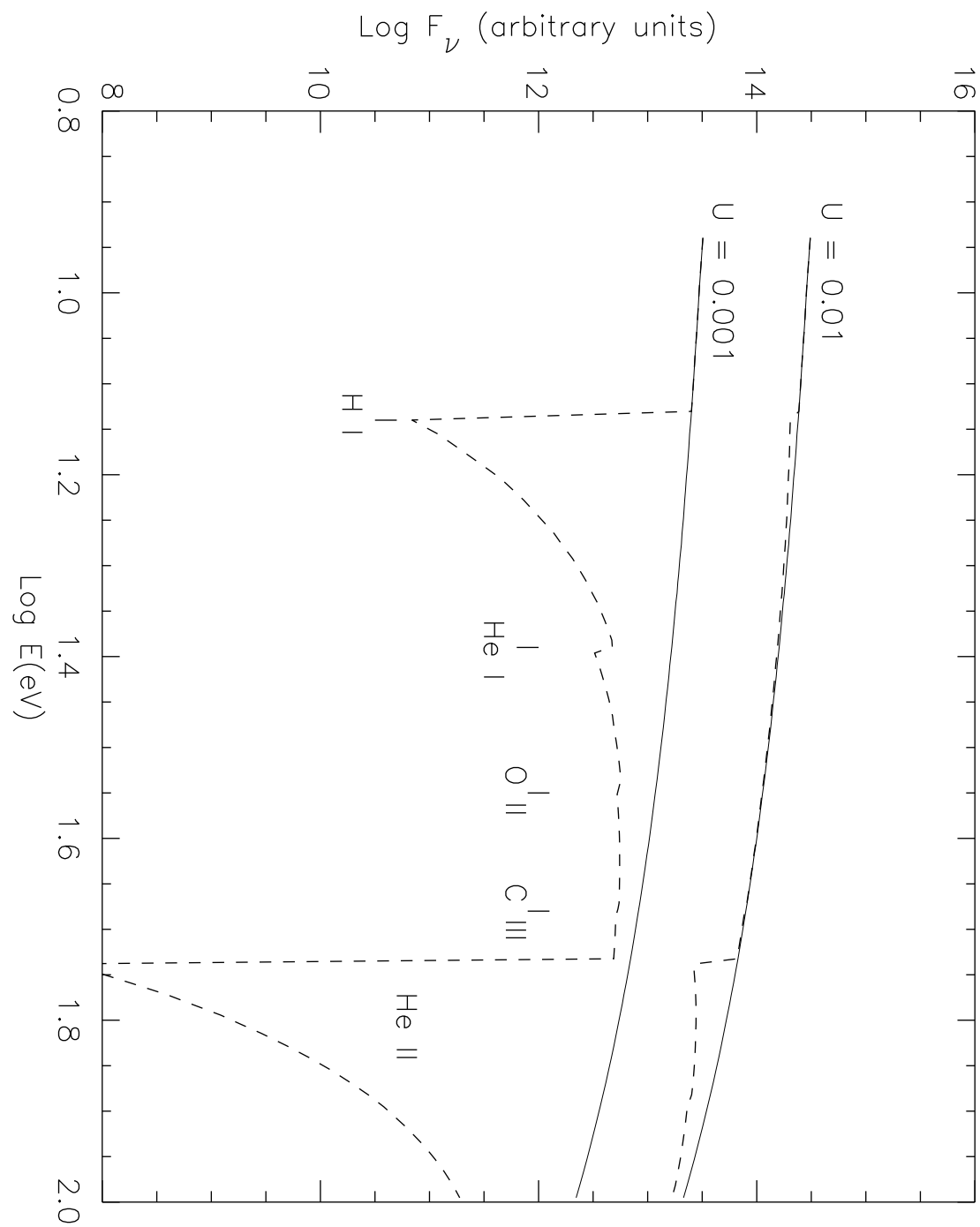
<sup>i</sup>ROSAT/PSPC (Nandra et al. 1995).

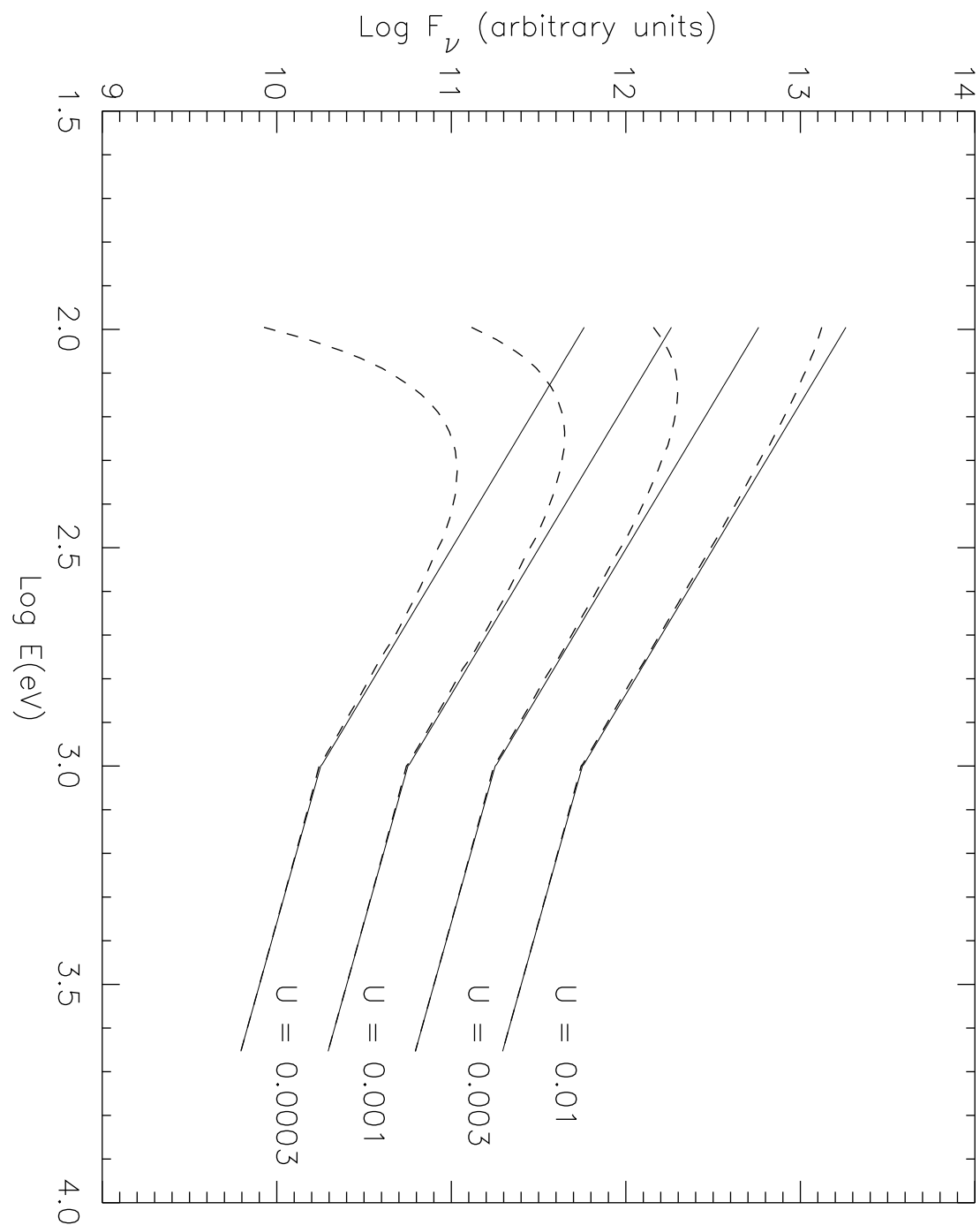
<sup>j</sup>SSS/MPC (Turner et al. 1991).

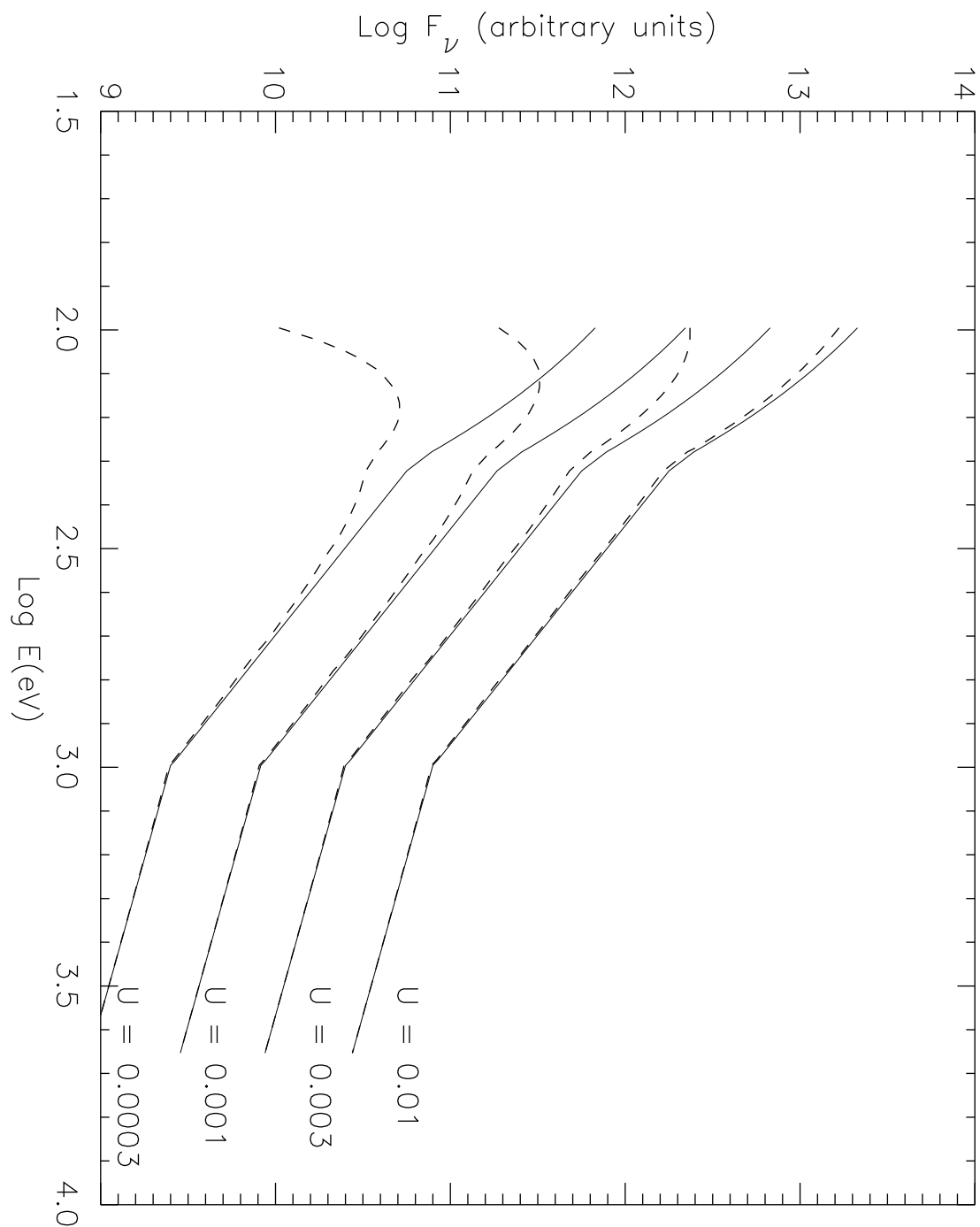
<sup>k</sup>fit between 1460Å , from *IUE* and 2 keV, from *Einstein* IPC, assuming an intrinsic  $\alpha = -1.0$  in the X-ray (Wilkes et al 1994).

<sup>l</sup>fit between 1375Å and 2 keV from values in Walter & Fink (1993) (see references therein).









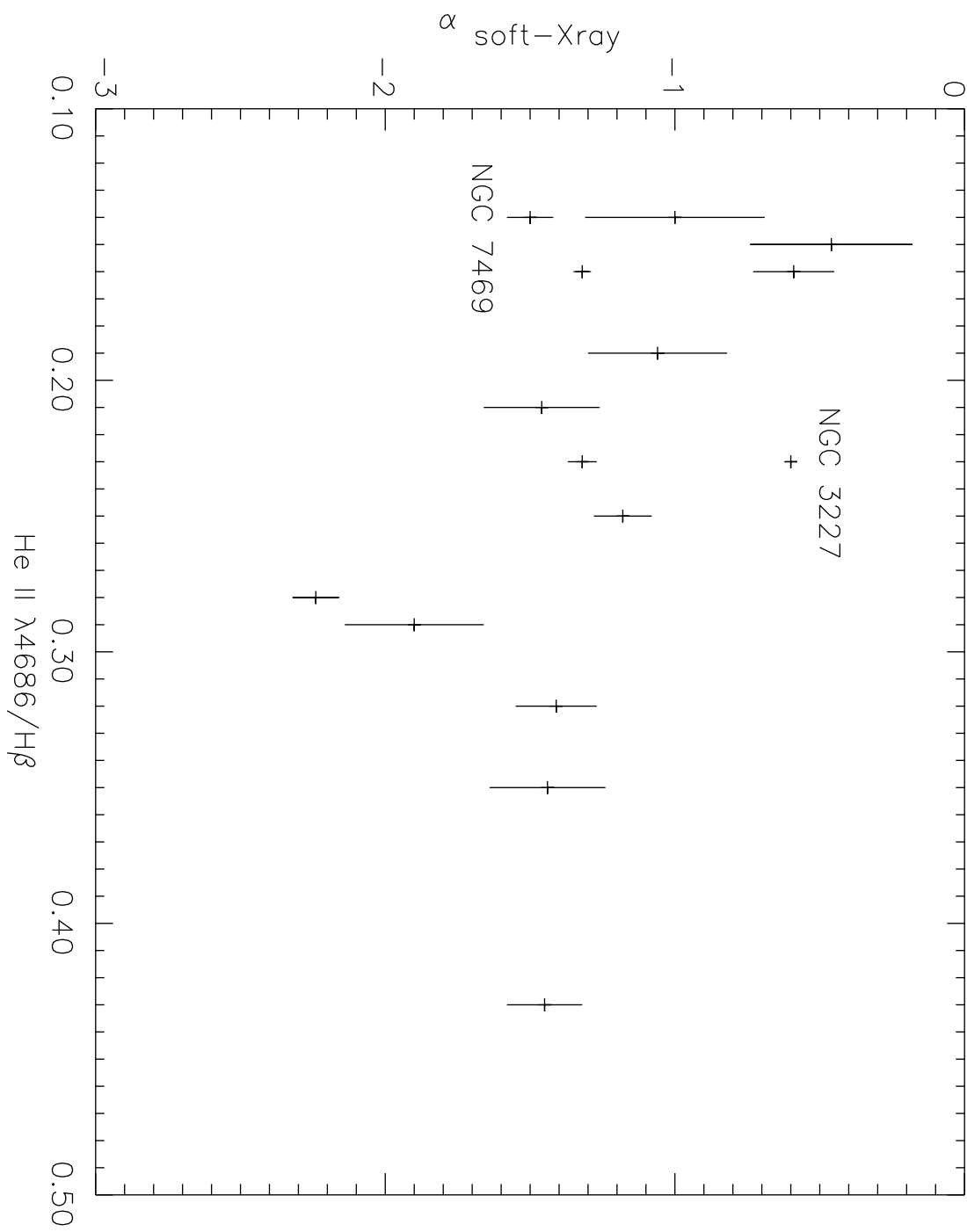


TABLE 1  
UV ABSORBER MODELS: IONIC COLUMN DENSITIES (IN UNITS OF  $10^{14}\text{cm}^{-2}$ ) AND FRACTION OF TRANSMITTED FLUX

$U_{abs}$	UV SED type	N(C IV)	N(N V)	N(O VI)	N(O VII)	N(Si IV)	N(Mg II)	$f_{13.8}$	$f_{54.7}$	$f_{105.5}$
$10^{-2.0}$	power-law	111.00	16.54	13.70	0.90	2.52	0.00	0.87	0.28	0.76
$10^{-2.5}$	power-law	66.19	1.89	0.51	0.01	9.84	0.15	0.56	0.002	0.31
$10^{-3.0}$	power-law	10.48	0.09	0.01	0.00	1.97	3.18	0.003	0.00	0.11
$10^{-3.5}$	power-law	0.40	0.00	0.00	0.00	0.03	7.67	0.00	0.00	0.03
$10^{-2.0}$	BBB	118.00	19.68	10.36	0.31	5.57	0.00	0.85	0.41	0.81
$10^{-2.5}$	BBB	87.04	2.29	0.43	0.00	12.62	0.15	0.52	0.009	0.41
$10^{-3.0}$	BBB	15.11	0.08	0.01	0.00	2.24	2.92	0.003	0.00	0.13
$10^{-3.5}$	BBB	0.53	0.00	0.00	0.00	0.02	8.54	0.00	0.00	0.03
$10^{-2.1}$	(NGC 4151) <sup>c</sup>	53.0	-	-	-	-	0.23	-	-	-

<sup>a</sup> $f_E$  is the ratio of the incident flux, at energy E eV, at the ionized face of the cloud to the residual flux at the point the model is truncated.

<sup>b</sup>Calculated ionization parameter for a “screened” NLR model:  $n_H = 10^5\text{cm}^{-3}$ ; for a cloud exposed to unattenuated central radiation,  $U_{nlr} = 10^{-2.5}$ .

<sup>c</sup>Observed ionic columns for Component 7, from Kriss (1998); predicted effective column,  $N_{eff} = 7.9 \times 10^{19}\text{cm}^{-2}$ .

TABLE 2  
LINE RATIOS (RELATIVE TO TO  $H\beta$ ) FROM NLR MODELS<sup>a</sup>, FOR THE POWER-LAW IONIZING CONTINUUM

	Unattenuated	Model 1 <sup>b</sup>	Model 1 <sup>c</sup>	Model 2 <sup>d</sup>	Model 2 <sup>e</sup>	Model 3 <sup>f</sup>	Model 3 <sup>g</sup>	Model 4 <sup>h</sup>
Ly $\alpha$ $\lambda$ 1216	39.41	39.49	39.50	40.34	40.49	54.13	63.96	71.61
C IV $\lambda$ 1550	0.74	0.50	0.47	0.32	0.29	2.23	3.77	3.30
C III] $\lambda$ 1909	2.50	2.23	2.19	1.99	1.94	5.45	7.60	8.29
C II] $\lambda$ 2326	1.21	1.21	1.21	1.27	1.28	2.21	2.64	2.94
[Ne IV] $\lambda$ 2423	0.20	0.14	0.13	0.07	0.06	0.25	0.28	0.58
Mg II $\lambda$ 2800	1.72	1.78	1.79	1.93	1.96	2.20	2.33	1.56
[Ne V] $\lambda$ 3426	0.09	0.06	0.05	0.02	0.02	0.10	0.08	0.38
[O II] $\lambda$ 3727	0.46	0.47	0.47	0.50	0.50	0.77	0.91	1.03
[Ne III] $\lambda$ 3869	1.36	1.40	1.41	1.51	1.53	2.55	3.21	2.59
[O III] $\lambda$ 4363	0.26	0.24	0.24	0.23	0.23	0.60	0.84	0.79

TABLE 2—Continued

	Unattenuated	Model 1 <sup>b</sup>	Model 1 <sup>c</sup>	Model 2 <sup>d</sup>	Model 2 <sup>e</sup>	Model 3 <sup>f</sup>	Model 3 <sup>g</sup>	Model 4 <sup>h</sup>
He II $\lambda$ 4686	0.21	0.15	0.15	0.09	0.07	0.18	0.16	0.31
H $\beta$	1.00	1.00	1.00	1.00	1.00	1.00	1.00	1.00
[O III] $\lambda$ 5007	17.41	17.33	17.31	17.37	17.29	28.50	34.15	30.67
[O I] $\lambda$ 6300	0.77	0.77	0.77	0.82	0.83	1.36	1.58	1.94
[N II] $\lambda$ 6548, 6584	1.38	1.41	1.41	1.50	1.51	2.47	2.99	3.54
H $\alpha$ $\lambda$ 6563	2.95	2.96	2.96	2.98	2.98	3.27	3.54	3.70
[S II] $\lambda\lambda$ 6716, 6731	0.13	0.13	0.12	0.12	0.12	0.09	0.08	0.06

<sup>a</sup>U<sub>nlr</sub> = 10<sup>-2.5</sup>, n<sub>H</sub>=1x10<sup>5</sup>cm<sup>-3</sup>, no dust, N<sub>eff</sub> = 10<sup>21</sup>cm<sup>-2</sup>

<sup>b</sup>U<sub>abs</sub> = 10<sup>-2</sup>, 90% covering

<sup>c</sup>U<sub>abs</sub> = 10<sup>-2</sup>, 100% covering

<sup>d</sup>U<sub>abs</sub> = 10<sup>-2.5</sup>, 90% covering

<sup>e</sup>U<sub>abs</sub> = 10<sup>-2.5</sup>, 100% covering

<sup>f</sup>U<sub>abs</sub> = 10<sup>-3</sup>, 90% covering

<sup>g</sup>U<sub>abs</sub> = 10<sup>-3</sup>, 100% covering

<sup>h</sup>U<sub>abs</sub> = 10<sup>-3.5</sup>, 90% covering

<sup>i</sup>U<sub>abs</sub> = 10<sup>-3.5</sup>, 100% covering

TABLE 3  
LINE RATIOS (RELATIVE TO TO  $H\beta$ ) FROM NLR MODELS<sup>a</sup>, FOR THE BBB IONIZING CONTINUUM

	Unattenuated	Model 1 <sup>b</sup>	Model 1 <sup>c</sup>	Model 2 <sup>d</sup>	Model 2 <sup>e</sup>	Model 3 <sup>f</sup>	Model 3 <sup>g</sup>	Model 4 <sup>h</sup>
Ly $\alpha$ $\lambda$ 1216	39.65	37.00	37.00	37.30	37.36	41.79	44.27	45.07
C IV $\lambda$ 1550	1.05	0.74	0.71	0.41	0.36	1.50	2.04	1.97
C III] $\lambda$ 1909	2.61	2.38	2.35	2.05	1.99	3.85	4.72	4.63
C II] $\lambda$ 2326	0.93	0.94	0.94	0.97	0.98	1.45	1.64	1.70
[Ne IV] $\lambda$ 2423	0.23	0.16	0.16	0.07	0.05	0.13	0.09	0.37
Mg II $\lambda$ 2800	1.87	1.96	1.97	2.15	2.18	2.67	2.95	1.80
[Ne V] $\lambda$ 3426	0.09	0.06	0.06	0.02	0.01	0.04	0.02	0.22
[O II] $\lambda$ 3727	0.38	0.38	0.38	0.40	0.41	0.52	0.57	0.60
[Ne III] $\lambda$ 3869	1.35	1.39	1.40	1.49	1.51	2.17	2.57	1.83
[O III] $\lambda$ 4363	0.27	0.26	0.25	0.24	0.23	0.45	0.56	0.45

TABLE 3—*Continued*

	Unattenuated	Model 1 <sup>b</sup>	Model 1 <sup>c</sup>	Model 2 <sup>d</sup>	Model 2 <sup>e</sup>	Model 3 <sup>f</sup>	Model 3 <sup>g</sup>	Model 4
He II $\lambda$ 4686	0.25	0.19	0.18	0.10	0.07	0.14	0.09	0.30
H $\beta$	1.00	1.00	1.00	1.00	1.00	1.00	1.00	1.00
[O III] $\lambda$ 5007	17.76	17.87	17.88	17.94	17.87	25.25	28.79	23.32
[O I] $\lambda$ 6300	0.37	0.38	0.38	0.40	0.41	0.63	0.71	1.04
[N II] $\lambda$ 6548, 6584	1.19	1.14	1.14	1.12	1.51	1.52	1.67	1.80
H $\alpha$ $\lambda$ 6563	2.92	2.92	2.92	2.93	2.93	3.02	3.08	3.06
[S II] $\lambda\lambda$ 6716, 6731	0.14	0.14	0.14	0.15	0.15	0.14	0.13	0.10

<sup>a</sup>U<sub>nlr</sub> = 10<sup>-2.5</sup>, n<sub>H</sub>=1x10<sup>5</sup>cm<sup>-3</sup>, no dust, N<sub>eff</sub> = 10<sup>21</sup>cm<sup>-2</sup>

<sup>b</sup>U<sub>abs</sub> = 10<sup>-2</sup>, 90% covering

<sup>c</sup>U<sub>abs</sub> = 10<sup>-2</sup>, 100% covering

<sup>d</sup>U<sub>abs</sub> = 10<sup>-2.5</sup>, 90% covering

<sup>e</sup>U<sub>abs</sub> = 10<sup>-2.5</sup>, 100% covering

<sup>f</sup>U<sub>abs</sub> = 10<sup>-3</sup>, 90% covering

<sup>g</sup>U<sub>abs</sub> = 10<sup>-3</sup>, 100% covering

<sup>h</sup>U<sub>abs</sub> = 10<sup>-3.5</sup>, 90% covering

<sup>i</sup>U<sub>abs</sub> = 10<sup>-3.5</sup>, 100% covering